The Conformers of Allyl-Isothiocyanate: A Combined Microwave Spectroscopy and Computational Study

Joseph Stitsky, Weslley G. D. P. Silva, Wenhao Sun and Jennifer van Wijngaarden*

Department of Chemistry, University of Manitoba, Winnipeg, Manitoba, R3T 2N2, Canada

*Corresponding Author

Email: vanwijng@cc.umanitoba.ca

Phone: (204)-474-8379

Fax: (204)-474-7608

Abstract

The pure rotational spectrum of allyl isothiocyanate (CH_2=$CHCH_2$-NCS) was collected from 4-26 GHz using Fourier transform microwave (FTMW) spectroscopy. Its analysis revealed the presence of two conformers that arise due to variation in the CCCN and CCNC dihedral angles. The observed spectrum is consistent with the accompanying potential energy surfaces derived using quantum chemical calculations at the B3LYP-D3(BJ) and MP2 levels of theory. Together, this experimental and theoretical study unequivocally identifies a new conformer (I) as the global minimum geometry. The spectral assignment of this new conformer is verified by the observation of transitions consistent with its ^{34}S, ^{13}C and ^{15}N isotopologues and with the characteristic ^{14}N quadrupole hyperfine patterns. For conformer I, the substitution (r_s) and effective ground state (r_0) structures were derived and reveal contributions from a large amplitude motion in the CCNC angle. The remaining geometric parameters compare well with the equilibrium structure (r_e) from B3LYP-D3(BJ)/cc-pVQZ calculations. The derived CNC bond angle of 152.6(3)^o for conformer I of allyl-NCS is found to be ~15^o larger than that of allyl-NCO (137.5(4)^o), which is in line with a change in the hybridization at nitrogen from an orbital with more ~sp character in allyl-NCS to ~$sp^{1.5}$ in allyl-NCO as determined via natural bond orbital analyses.

Introduction

The detection of gas phase NCO- and NCS-containing compounds in molecular clouds through the identification of their spectral fingerprints provides useful information for modelling the chemistry of the interstellar medium. Aided by laboratory-based high resolution rotational spectroscopy, the existence of HNCO,[1] HNCS,[2] HOCN,[3,4] HSCN[5,6] and CH_3NCO[7,8] in space have already been confirmed making the study of other NCO/NCS containing species of astronomical interest. Organic isothiocyanates, such as allyl-NCS (Fig. 1), are naturally occurring in plant cells where they are produced as a result of cellular damage,[9] and also have industrial applications such as in food preservation.[10] This class of compounds, therefore, is of broad chemical interest as components of diverse systems in both terrestrial and astronomical environments.

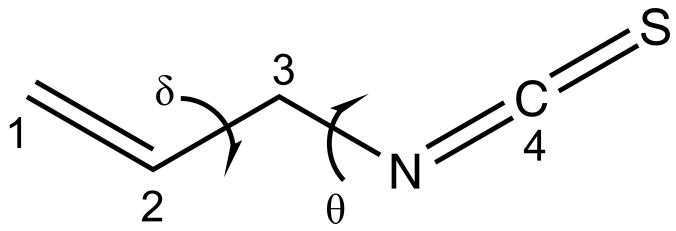

Fig. 1. Chemical structure of allyl-NCS showing dihedral angles δ (C_1-C_2-C_3-N) and θ (C_2-C_3-N-C_4). Both δ and θ are 180° in this image.

When compared to previously studied NCO/NCS-containing molecules, the allyl-substituted compounds present a more complex conformational landscape due to the additional methylene (CH_2) group in their backbone.[11] The rotational spectrum of allyl-NCO, for example, has been a puzzle in the literature for more than twenty-five years. Although two stable conformations, *cis* (δ= 0º and θ=180º) and *gauche* (δ= ~120º and θ=0º) were predicted, only the higher energy *gauche* conformer was observed via its rotational spectrum.[12,13] Recently, an accurate picture of the conformational space of allyl-NCO was derived by exploiting high-resolution Fourier transform microwave (FTMW) spectroscopy and dispersion-corrected density

functional theory (DFT-D) calculations.[11] In addition to the previously reported *gauche* conformer, transitions consistent with a new global minimum geometry (conformer I) were observed. The derived potential energy surface furthermore confirmed that the *cis* conformer could undergo facile relaxation to conformer I in the molecular beam expansion.

In allyl-NCO,[11] the intramolecular dispersive interaction between the CH_2=CH- and NCO-groups was found to play a critical role in the conformational distribution as it led to the existence of conformer I. From previous spectroscopic reports involving allyl-NCS, the conformational story appears to mimic that found in the earlier studies of its oxygen analog. Using Stark-modulated microwave spectroscopy,[14,15] a *gauche* conformer was reported for allyl-NCS while a purported lower energy *cis* conformer based on ^{13}C NMR experiments[16] was not observed. Based on this, it is clear that the conformational space of allyl-NCS requires further study to explore whether a new, dispersion-stabilized conformer is present and how the change from oxygen to sulfur influences the conformational equilibrium.

Rotational studies on isocyanates and isothiocyanates, in general, not only identify stable conformers, but also afford the opportunity to investigate the influence of the terminal chalcogen atom on the electronic environment around the nitrogen atom. Comparison of the geometries of HCCNCO[17] and HCCNCS,[18] for example, have shown that changing from oxygen to sulfur results in an increase in the CNC bond angle from 140.7º to 180º. In the phenyl (Ph) containing analogues,[19] the difference in the CNC bond angle increases by a smaller amount (~10º) from 135.2º in PhNCO to 145.1º in PhNCS which is related to a change in the hybridization at nitrogen from a ~$sp^{1.6}$- to a ~sp-hybridized orbital in these two compounds, respectively. Exploring related pairs of compounds with different R groups will provide greater insight into the role of the R substituent and terminal chalcogen on the electronic structures of NCO/NCS-containing species.

Herein, a detailed investigation of the conformational landscape of allyl-NCS is reported through a combination of Fourier transform microwave (FTMW) spectroscopy in a supersonic jet expansion and quantum mechanical calculations. Guided by the construction of potential energy surfaces that account for dispersive interactions, transitions due to two distinct conformers were observed in the rotational spectrum. This includes the first assignment of the new global minimum geometry, conformer I. In addition to hyperfine structure due to the ^{14}N quadrupole nucleus, transitions from minor isotopologues of all heavy atoms (^{13}C, ^{15}N and ^{34}S) were observed in natural abundance for conformer I allowing experimental geometries to be derived. Differences in the conformational equilibrium of allyl-NCO and allyl-NCS are discussed as are changes in the geometry of conformer I by comparing the derived potential energy surfaces and results from natural bond orbital analyses.

Experimental Methods

The rotational spectrum of allyl-NCS (Sigma-Aldrich, 94%, bp: 150°C) was collected using a chirped pulse (cp) and a Balle-Flygare Fourier transform microwave (FTMW) spectrometer, both of which have been described previously.[20,21] Briefly, a gas mixture was prepared containing ~1% allyl-NCS in neon buffer gas and delivered to the high vacuum chamber through a pulsed nozzle. The resulting supersonic jet expansion cools the sample to a rotational temperature of ~5 K thereby favoring low energy conformations. Initially, a broadband spectrum was recorded from 8-18 GHz in segments of 2 GHz using the cp-FTMW spectrometer. Rotational transitions belonging to the parent species of two conformers, later determined to be conformers I and III (see Computational Methods below), were assigned in addition to those of their minor heavy isotopologues (^{13}C, ^{15}N, and ^{34}S) in natural abundance. A 3 GHz portion of the cp-FTMW

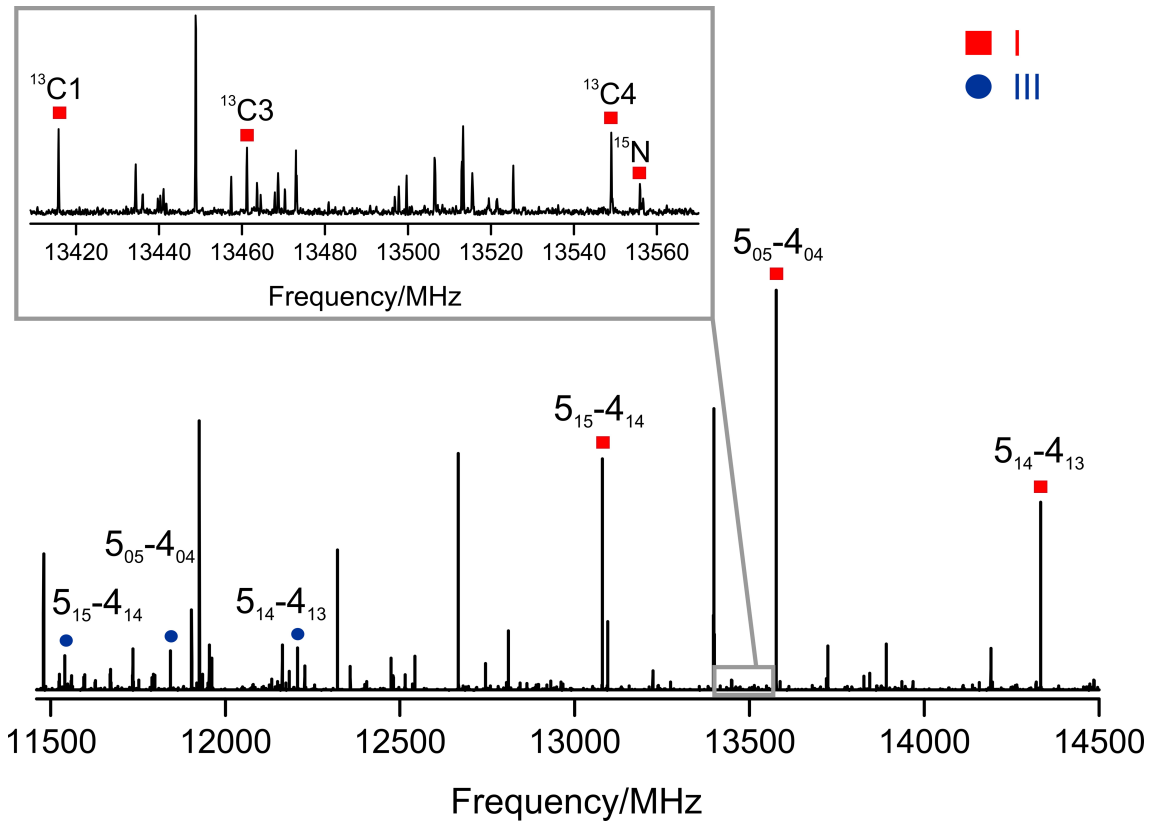

Fig. 2. Sample 3 GHz segment of the cp-FTMW spectrum. The 5_{05}-4_{04} rotational transitions due to ^{13}C and ^{15}N species of conformer I are shown in the enhanced portion of the spectrum. (3 million FIDs).

spectrum is shown in Fig. 2. Following initial assignment of the survey spectrum, final measurements were done using the Balle-Flygare FTMW spectrometer from 4-26 GHz in order to resolve the hyperfine structure due to the presence of the ^{14}N nucleus as well as lower intensity transitions that were not observed in the cp-FTMW data. A sample transition recorded using the cavity-based FTMW instrument is shown in Fig. 3. Transitions recorded using this higher resolution spectrometer appear as doublets due to the Doppler effect as a result of the collinear nature of the resonator axis and the jet expansion. Individual components have line widths of approximately 7 kHz (FWHM) and the line positions are determined to roughly ±2 kHz.

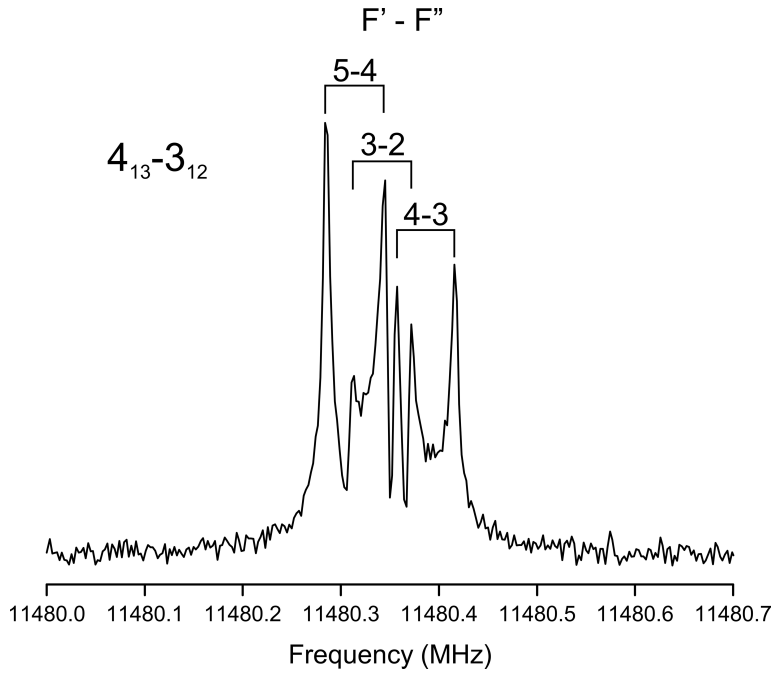

Fig. 3. Sample Balle-Flygare FTMW spectrum (410 cycles) showing the 4_{13}-3_{12} rotational transition of conformer I including the ^{14}N hyperfine structure.

Computational Methods

The energy minima of allyl-NCS were first identified through the construction of three-dimensional potential energy surfaces (PES) created by scanning both the dihedral angles δ and θ in 36 steps of 10° while allowing all other parameters to relax. These scans were conducted using density functional theory (DFT) and second order Møller-Plesset perturbation theory (MP2)[22] calculations with the Gaussian 16 Revision B.01 software.[23] For the DFT calculations, we tested the popular B3LYP[24,25] method along with its B3LYP-D3(0) and B3LYP-D3(BJ) versions, which include Grimme's dispersion corrections with the zero-damping and Becke-Johnson damping schemes,[26,27] respectively. All initial calculations were carried out using the cc-pVTZ basis set.[28–30] The PES obtained are shown in Fig. 4. In the end, five energy minima, which resemble the ones reported for allyl-NCO,[11] were identified from the PES scans and were then fully optimized using

both B3LYP-D3(BJ) and MP2 methods with the cc-pVTZ and cc-pVQZ basis sets. To verify the nature of the stationary points and to compute the electronic energies with zero-point energy (ZPE) corrections, harmonic frequency calculations were also carried out for these minima at the same levels of theory. The optimized geometries corresponding to the five minima are depicted in Fig. 5 while their calculated relative energies, rotational constants and dipole moments calculated using the cc-pVQZ basis set are shown in Table 1.

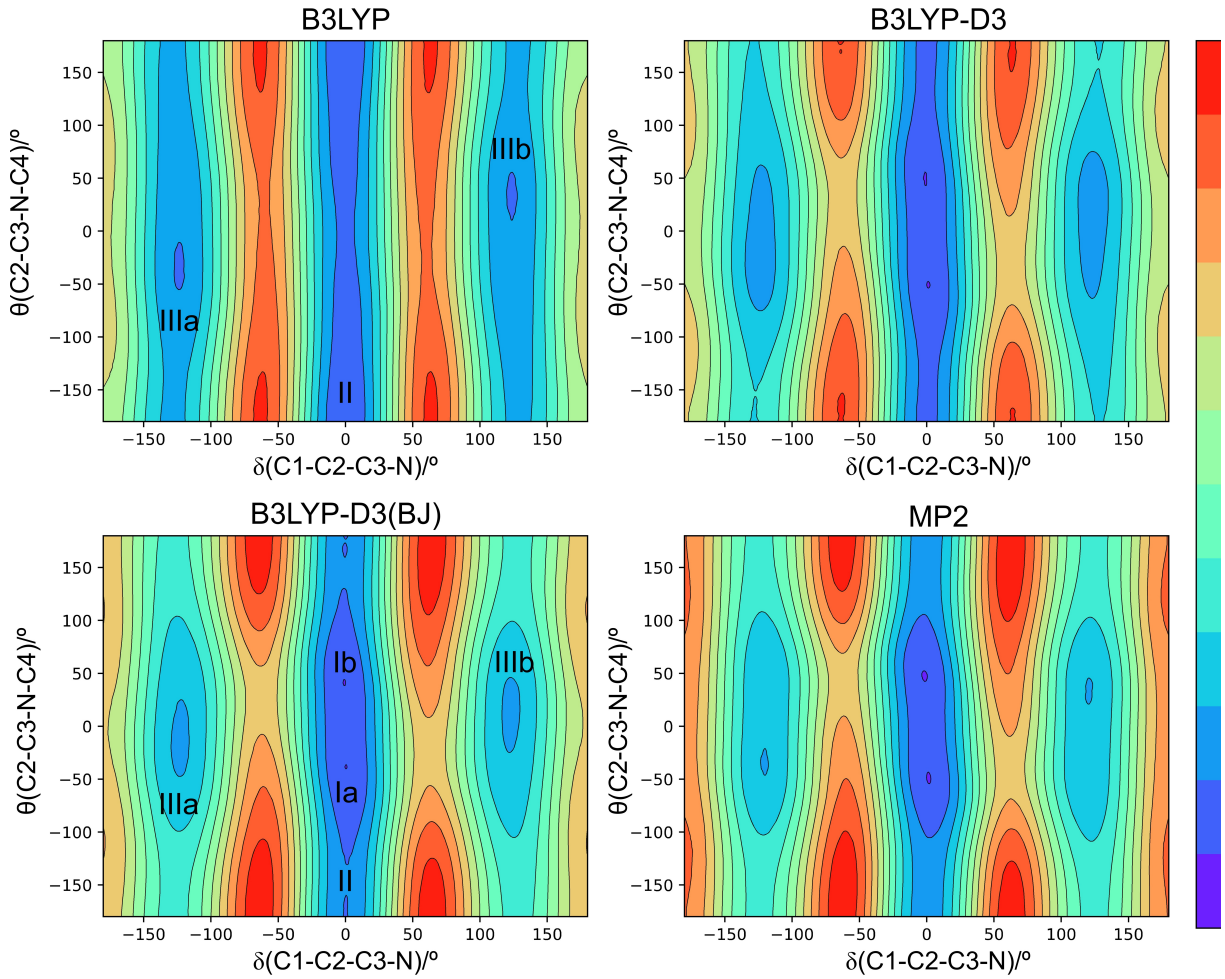

Fig. 4. Three-dimensional potential energy surfaces of allyl-NCS obtained by scanning the dihedral angles δ and θ at the B3LYP, B3LYP-D3, B3LYP-D3(BJ) and MP2 methods with the cc-pVTZ basis set. The relative energies are plotted in units of kJ mol^{-1}.

In Fig. 5, the conformers are labeled using Roman numerals from I to III to represent their order of stability with I being the lowest energy geometry. It is worth mentioning that conformers II and III correspond to the *cis* and *gauche* conformers, respectively, previously reported in the literature.[14] As conformers Ia/Ib and IIIa/IIIb are pairs of enantiomers, they present the same rotational and energetic parameters and thus, they are not distinguished in Table 1.

For B3LYP-D3(BJ) calculations, we also tested the performance of different basis sets from the Dunning's family in reproducing the experimental rotational constants for conformer I, detected here for the first time, and the results are summarized in Table S1. The basis sets (cc-pVXZ, cc-pV(X+d)Z, aug-cc-pVXZ, aug-cc-pV(X+d)Z where X= D, T, Q) chosen vary from double- to quadrupole-zeta and include those with and without additional polarization functions to describe the larger sulfur atom and diffuse functions to account for weak dispersive interactions. Surprisingly, with the exception of the double-zeta basis sets, no significant variations were observed among the results obtained with the triple- and quadrupole-zeta basis sets which

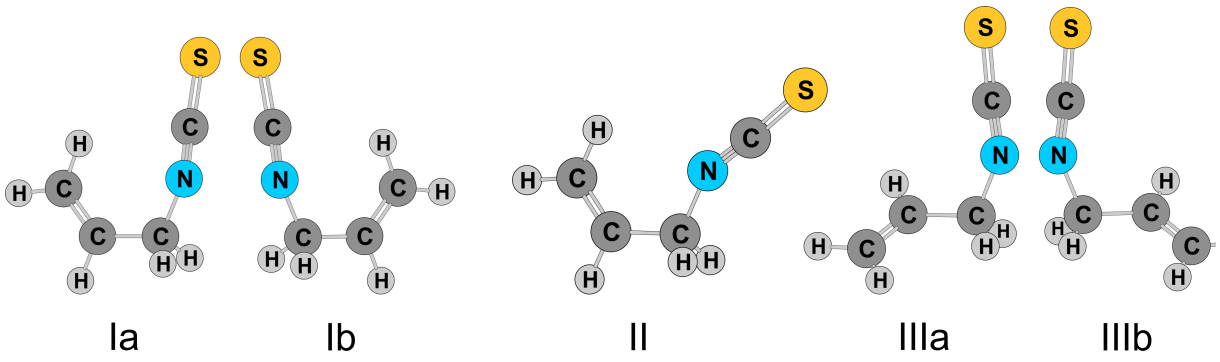

Fig. 5. Five optimized geometries corresponding to energy minima of allyl-NCS obtained at the B3LYP-D3(BJ)/cc-pVQZ level of theory. These geometries correspond to conformers Ia/Ib (δ = 0.9°/-0.9, θ = -43.2°/43.2°), II (δ = -0.3°, θ = 180.0°) and IIIa/IIIb (δ = -122.9°/122.9°, θ = -16.9°/16.9°). The Cartesian coordinates for all conformers are provided in Tables S1-S3 in the supporting information (SI) file.

Table 1. Calculated Relative Energies, Relative Populations, Equilibrium Rotational Constants and Dipole Moment Components for the Conformers of Allyl Isothiocyanate.

Constants	I		II		III	
	B3LYP-D3(BJ)	MP2	B3LYP-D3(BJ)	MP2	B3LYP-D3(BJ)	MP2
ΔE^a/kJ mol^{-1}	0.0	0.0	1.6	2.4	2.6	3.4
$P_{\Delta E}{}^b$/%	53.4	61.0	28.0	23.1	18.6	15.9
$\Delta E_{ZPE}{}^c$/ kJ mol^{-1}	0.0	0.0	1.0	1.7	2.5	3.3
$P_{\Delta EZPE}{}^d$/%	49.1	56.8	32.9	28.0	18.0	15.2
A/MHz	7018	7052	12176	11799	8373	8816
B	1488	1505	1121	1138	1229	1210
C	1245	1260	1033	1045	1108	1101
P_{aa} /amu Å^2	337	333	449	442	404	410
P_{bb}	69.2	68.5	40.0	41.2	52.6	49.3
P_{cc}	2.86	3.19	1.55	1.66	7.73	7.99
$\|\mu_a\|$/D	3.3	3.3	2.9	3.0	3.3	3.3
$\|\mu_b\|$	0.7	0.7	1.4	1.3	0.5	0.5
$\|\mu_c\|$	0.3	0.4	0.0	0.1	0.3	0.4

[a]Electronic energy relative to the most stable conformer I; [b]Relative population at 298K based on the electronic energies; [c]Electronic energy with zero-point energy (ZPE) corrections relative to the most stable conformer I; [d]Relative population at 298K based on the electronic energies with ZPE corrections.

reproduced the experimental rotational constants to within 0.7%. Similar results were observed in the benchmark study of allyl-NCO.[11]

Given the possibility of conformational changes during supersonic jet expansion, interconversion pathways were also calculated by scanning either the δ or θ dihedral angle in 36 steps of 10° at the B3LYP-D3(BJ)/cc-pVQZ level of theory for comparison with those of allyl-NCO.[11] During the scans, all other geometric parameters were allowed to relax. The calculated relaxation pathways are shown in Fig. 6. To obtain more accurate barriers for the interconversion of conformers along these pathways, the transition state points located on the PES were fully optimized at the B3LYP-D3BJ/cc-pVQZ level. Frequency calculations within the harmonic approximation at the same level of theory confirm the nature of the transition state geometries which exhibit one imaginary frequency. Finally, to examine differences in the electronic

environment of allyl-NCS and allyl-NCO, natural bond orbital (NBO) calculations were done for both molecules at the B3LYP-D3(BJ)/cc-pVTZ level using the NBO 6.0 program.[31]

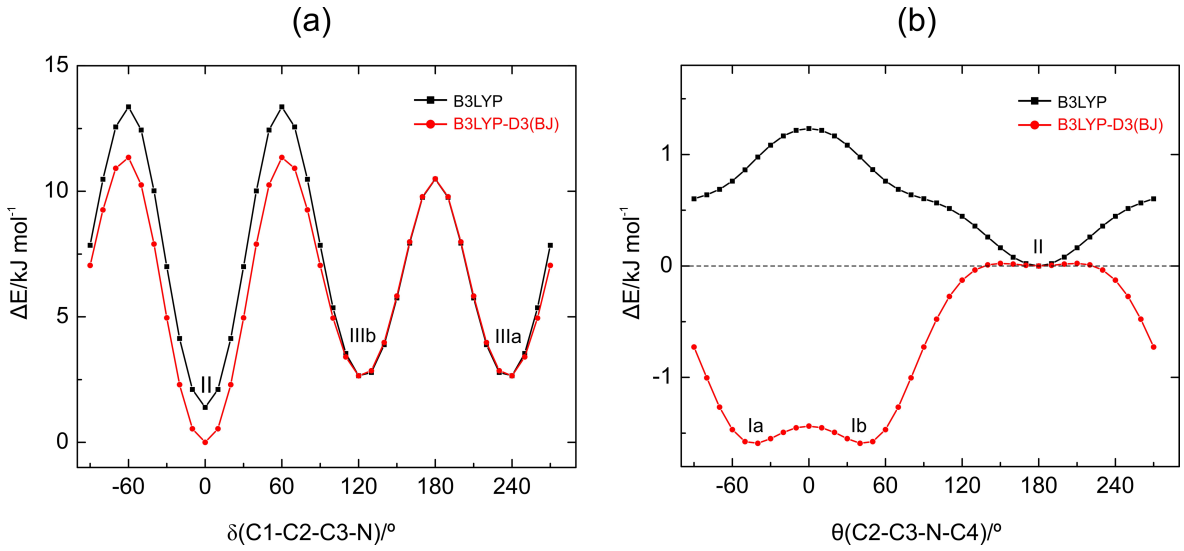

Fig. 6. a) Relaxation pathway calculated as a result of scanning the dihedral angle δ in 36 steps of 10° at the B3LYP/cc-pVQZ and B3LYP-D3(BJ)/cc-pVQZ levels of theory. b) Relaxation pathway calculated when scanning the dihedral angle θ in 36 steps of 10°, where the initial value of δ is 0°, at B3LYP/cc-pVQZ and B3LYP-D3(BJ)/cc-pVQZ levels of theory.

Spectral Analysis

Two sets of R-branch *a*- and *b*-type rotational transitions belonging to two different species with sizeable $|\mu_a|$ and $|\mu_b|$ permanent electric dipole moment components were assigned in the rotational spectrum of allyl-NCS. By comparing the experimental rotational constants with those predicted in Table 1, the transitions were attributed to the parent species of conformers I and III. In total, 96 (79 *a*- and 17 *b*-type) and 68 (53 *a*- and 15 *b*-type) hyperfine components were measured for conformers I and III, respectively. Despite accurate frequency predictions, no *c*-type transitions were observed which is consistent with the smaller values of $|\mu_c|$ (Table 1). For both

conformers, transitions corresponding to the singly substituted ^{34}S isotopologue in natural abundance were assigned and as the spectral features of conformer I dominate the spectrum in Fig. 2, there was sufficient intensity to assign transitions due to its ^{13}C and ^{15}N isotopologues. The measured transitions for each species were fit with Pickett's SPFIT program[32] using Watson's S-reduced Hamiltonian in the I^r representation.[33] During the spectral analysis, the parameters that were not well-determined were fixed to either the calculated values or to the corresponding parent values. The resulting spectroscopic constants are shown in Tables 2 and 3 while the lists of observed transitions are shown in Tables S2-S10 in the SI.

Following the determination of accurate rotational constants in Table 2 for the isotopologues of conformer I, the experimental geometry of its heavy atom framework was derived using Kisiel's STRFIT program[34] to fit the effective moments of inertia to a set of geometric parameters. This procedure was carried out by fixing the equilibrium positions of hydrogen atoms to those derived at the B3LYP-D3(BJ)/cc-pVQZ level of theory. The derived r_0 structure successfully reproduced the 21 experimental rotational constants of conformer I of allyl-NCS to within 0.011%. The heavy atom internal coordinates are summarized in Table 4 along with those of conformer I of allyl-NCO.[11] The corresponding parameters for the substitution structure (r_s) based on Kraitchman's equations[35] including Costain errors[36] as implemented in Kisiel's KRA program,[34] equilibrium geometry (r_e) and transition state (r_{ts}) for the interconversion between the conformer pair (Ia/Ib) are also provided. For the r_s structure, the c-coordinate of C1 was set to zero as the Kraitchman equations yielded an imaginary number due to its proximity to the ab-plane and signs of the coordinates were inferred from the r_e structure. The principal atomic coordinates for all four geometries (r_e, r_{ts}, r_0 and r_s) are available in the accompanying SI.

Table 2. Ground State Spectroscopic Constants Obtained for the Parent, ^{34}S, ^{13}C and ^{15}N Species of Conformer I.

	B3LYP-D3(BJ)[a]	Parent	^{34}S	^{13}C1	^{13}C2	^{13}C3	^{13}C4	^{15}N
Rotational Constants /MHz								
A	7018.38	6974.18615(71)	6958.4085(10)	6778.019(16)	6967.775(28)	6869.616(27)	6959.964(16)	6888.2007(91)
B	1488.33	1500.19662(12)	1456.87719(27)	1485.94460(26)	1476.20010(41)	1488.88154(36)	1497.20146(21)	1499.98257(13)
C	1245.07	1248.49890(11)	1217.88160(23)	1232.27174(25)	1231.70608(36)	1237.31331(31)	1245.99526(21)	1245.80534(13)
Centrifugal Distortion Constants /kHz								
D_J	1.12	1.05815(66)	0.9960(19)	1.0745(14)	1.0280(20)	1.0110(27)	1.0550(12)	1.04974(77)
D_{JK}	-4.43	-3.3149(53)	-3.124(10)	-3.630(10)	-3.598(29)	-2.440(16)	-3.4702(80)	-3.4799(47)
D_K	49.06	[49.06][b]	[49.06][b]	[49.06][b]	[49.06][b]	[49.06][b]	[49.06][b]	[49.06][b]
d_1	-0.35	-0.32019(90)	-0.2957(27)	-0.3260(23)	-0.3057(44)	-0.3090(38)	-0.3176(18)	-0.3208(11)
d_2	-0.04	-0.03868(48)	[-0.0387][c]	[-0.0387][c]	[-0.0387][c]	[-0.0387][c]	[-0.0387][c]	[-0.0387][c]
^{14}N Quadrupole Coupling Constants /MHz								
3/2 χ_{aa}	2.82	2.7147(21)	2.7292(78)	2.6999(60)	2.710(11)	2.7490(92)	2.7087(44)	-
1/4 (χ_{bb}-χ_{cc})	-0.03	-0.03094(79)	[-0.0309][c]	[-0.0309][c]	[-0.0309][c]	[-0.0309][c]	[-0.0309][c]	-
rms /kHz	-	1.4	1.5	1.4	1.7	1.5	1.4	0.5
# lines	-	97	49	43	42	36	59	22

[a]Dunning's cc-pVQZ basis set used. [b]Value fixed that from the quantum chemical calculation. [c]Value fixed to that derived for the parent isotopologue.

Table 3. Ground State Spectroscopic Constants Obtained for the Parent and ^{34}S Species of Conformer III.

	B3LYP-D3(BJ)[a]	Parent	^{34}S
Rotational Constants /MHz			
A	8372.97	8045.40393(50)	8011.01(22)
B	1228.71	1254.99398(11)	1221.74385(33)
C	1107.68	1121.603769(98)	1094.11081(40)
Centrifugal Distortion Constants /kHz			
D_J	2.20	2.10210(87)	2.1062(31)
D_{JK}	-78.53	-63.831(12)	-64.225(29)
D_K	908.24	[908.24][b]	[908.24][b]
d_1	-0.55	-0.52318(89)	-0.3965(32)
d_2	-0.01	-0.01443(63)	[-0.0144][c]
^{14}N Quadrupole Coupling Constants /MHz			
3/2 χ_{aa}	2.92	2.7908(32)	2.825(35)
1/4 (χ_{bb}-χ_{cc})	-0.12	-0.1037(11)	[-0.104][c]
rms /kHz	-	1.5	1.6
no. lines	-	68	24

[a]Dunning's cc-pVQZ basis set used. [b]Value fixed that from the quantum chemical calculation. [c]Value fixed to that derived for the parent isotopologue.

Table 4. Comparison of the Equilibrium (r_e) (B3LYP-D3(BJ)/cc-pVQZ)[a] and Effective Ground State (r_0) Geometries for Conformer I of Allyl-NCS and Allyl-NCO and Transition State Geometry (r_{ts}) for Ia/Ib Interconversion of Allyl-NCS (B3LYP-D3(BJ)/cc-pVQZ

	Allyl-NCS				Allyl-NCO[b]	
	r_e[b]	r_s	r_0	r_{ts}	r_e[b]	r_0
C_2-C_1	1.323	1.347(7)	1.339(5)	1.322	1.323	1.341(11)
C_3-C_2	1.504	1.495(6)	1.504(5)	1.504	1.502	1.498(10)
N-C_3	1.424	1.529(16)	1.429(7)	1.420	1.438	1.453(22)
C_4-N	1.184	1.081(14)	1.178(7)	1.181	1.197	1.189(14)
S/O-C_4	1.583	1.594(4)	1.583(4)	1.585	1.170	1.171(13)
∠ C_3-C_2-C_1	126.4	125.6(3)	125.8(2)	126.6	126.6	125.8(3)
∠ N-C_3-C_2	114.8	115.3(3)	114.5(3)	115.2	115.2	115.1(5)
∠ C_4-N-C_3	150.7	148.9(11)	152.6(3)	154.3	138.8	137.5(4)
∠ S/O-C_4-N	176.1	173.0(14)	[176.1][c]	176.3	173.4	[173.4][c]
τ N-C_3-C_2-C_1	0.86	-1.3(39)	[0.86][c]	0.0	0.4	[0.4][c]
τ C_4-N-C_3-C_2	-43.2	-32(5)	-33.9(4)	0.0	-58.9	-57.8(8)
τ S/O-C_4-N-C_3	178.6	178(17)	[178.6][c]	180.0	179.9	[179.9][c]

[a]Dihedral angles consistent with Ia enantiomer; [b]Reference 11; [c]Parameters held fixed to equilibrium values.

Discussion

The exploration of the conformational landscape of allyl-NCS through the construction of three-dimensional PES led to the identification of five energy minima reported in Fig. 5. By comparing the PES obtained at the different levels (Fig. 4), one can see that standard B3LYP calculations fail to identify conformer I as an energy minimum, while the dispersion-corrected DFT and MP2 methods find all three conformers of allyl-NCS. The absence of conformer I in the B3LYP PES is related to the inability of this computational method to describe the attractive dispersive π···π interaction between the thiocyanato (-N=C=S) and the allyl (-CH=CH_2) group. The importance of dispersion corrections in obtaining an accurate picture of the conformer landscape has been reported for other systems including those with only first row elements such

as methyl jasmonate and zingerone.[37] Similar results were observed in the benchmark study of the PES of the isovalent allyl-NCO compound, where among more than 20 functionals tested, dispersion uncorrected DFT methods failed to describe the proper conformational distribution.[11] Thus, although allyl-NCS was investigated previously using both computational[16,38] and experimental[14,15,16] methods, the present work is the first study to predict and confirm the presence of conformer I, the lowest energy conformation.

From the intensities of the observed transitions in Fig. 1 and considering that conformers I and III are predicted to have similar $|\mu_a|$ and $|\mu_b|$ values (Table 1), conformer I is the dominant species in the spectrum. Based on the calculated populations at 298K (Table 1), conformer II is predicted to be more stable than III but no transitions attributable to this geometry were assigned. It has been shown empirically that in a cold rare gas jet, higher energy conformers undergo relaxation to lower energy forms when the interconversion barrier is lower than ~4.8 kJ/mol.[39] This empirical rule of thumb has been used to justify the absence of conformers in other systems with alkane backbones such as perillyl alcohol where eight of 12 low energy conformers persisted in the jet.[40] By analyzing the relaxation pathway from II→I for allyl-NCS (Fig. 6b) the calculated interconversion barrier is only ~0.02 kJ/mol (0.05 kJ/mol with ZPE corrections)(B3LYP-D3(BJ)/cc-pVQZ) which implies that conformer II will relax to conformer I in the expansion. For comparison, the barrier is smaller than that reported for allyl-NCO (0.13 kJ/mol with ZPE) at the same level of theory which was used to justify the lack of features arising from conformer II in its microwave spectrum.[11] Such a flat PES along the δ=0 coordinate calls into question whether the ZPE corrections, based on harmonic vibrations, are valid but nevertheless, conformer II was a true minimum on the PES of allyl-NCS tested at the B3LYP-D3(BJ) (cc-pVQZ, aug-cc-pVTZ, aug-cc-pVQZ) and MP2 (cc-pVQZ, aug-cc-pVTZ) levels based on the absence of imaginary frequencies.

The fact that conformer II was not observed in a static gas sample[14,15] certainly calls into question whether this is a stable conformer.

Although conformers I and III exist as pairs of enantiomers (Ia/Ib and IIIa/IIIb) which are equivalent minima on the PES, no tunnelling splitting related to their interconversion was observed. This was surprising initially as a tunnelling splitting was reported for the transitions of conformer I in allyl-NCO.[11] To understand this, the heights of the energy barriers associated with the interconversion between the enantiomer pairs of I and III were evaluated from the potential energy curves in Fig. 6. The barrier between Ia and Ib (Fig. 6b) is calculated to be ~0.15 kJ/mol, but when accounting for ZPE corrections, the energy difference between conformer I and the transition state is lowered to -0.17 kJ/mol. This indicates that the interconversion between Ia and Ib is barrierless in allyl-NCS and is consistent with the observed spectra in which *c*-type transitions are not observed. For comparison, in allyl-NCO,[11] the ZPE-corrected interconversion barrier in conformer I is higher (~0.8 kJ/mol) which supports the observation of tunnelling splitting. Conversely, for conformer III of allyl-NCS, the relatively high energy barrier between IIIa and IIIb (Fig. 6a) of 7.88 kJ/mol is expected to quench tunnelling and this barrier is comparable to that reported for conformer III of allyl-NCO (7.86 kJ/mol).[11]

To better rationalize why the enantiomeric interconversion barrier is larger by ~1 kJ/mol for conformer I of allyl-NCO compared with that of allyl-NCS (while those of conformers III are nearly identical before ZPE correction), we investigated the potential energy curves for the Ia/Ib tunnelling pathway for allyl-NCS in Fig. 6b with the analogous profile for allyl-NCO in reference 11. By analyzing the B3LYP energy (without the inclusion of dispersive corrections), one can see that the transition state structure (C-C-N-C= 0º) of allyl-NCO already lies ~1 kJ/mol higher in energy than that of allyl-NCS (when referenced to conformer II in each case). From the geometry

of the transition states as shown in Fig. S1 of the SI, we assert that this higher barrier is related to steric repulsion as the allyl and isocyanato groups are in closer proximity in allyl-NCO. When dispersion corrections are included, the Ia/Ib interconversion barrier is retained in allyl-NCO but the motion is barrierless in allyl-NCS.

The substitution (r_s) and effective ground state (r_0) geometries of conformer I in Table 4 are in good agreement within the derived uncertainties of each method with the precision of the former limited by relatively large Costain errors in the coordinates of atoms close to inertial axes. The Costain errors are meant to account for vibrational effects[36] and the resulting uncertainties in the r_s parameters, particularly the dihedral angles, is consistent with the influence of a large amplitude motion such as that required for interconversion of the Ia/Ib enantiomer pair as seen in Figure 6. Thus, it is evident that the experimental rotational constants used to derive the r_s and r_0 geometries involve contributions from this barrierless motion and should be interpreted with caution. It is worth noting that comparison of the r_0, equilibrium (r_e) and transition state (r_{ts}) geometries in Table 4 reveals that most parameters actually match to within 2σ. The largest discrepancy is found in the dihedral angle τ(C4-N-C3-C2) (θ) that corresponds to this large amplitude motion with the value obtained from experiment (-33.9(4)°) (where the negative sign refers to conformer Ia) falling between those calculated for the global minimum (-43.2°) and the transition state (0°). This occurs because the effective ground state rotational constants used to derive the experimental geometries are expectation values that depend on the squares of distances through the moments of inertia such that the contributions from the positive and negative motions along θ do not cancel. A similar explanation was invoked to rationalize the spectrum of 2-fluoroethanol···H_2O as arising from an intermediate geometry of two low-lying conformers (I and II) that interconvert.[41] Furthermore, for allyl-NCS, the r_s geometry provides a second estimate of

the θ dihedral angle (-32(5)^{o}) that is independent of *a priori* assumptions from quantum chemical calculations (beyond the signs of the individual coordinates). One can more directly observe the effects of large amplitude motions over θ for conformer I of allyl-NCS through investigation of the planar moments. Using the rotational constants for the parent isotopologue of conformer I from Table 2, P_{cc} is 2.28 amu Å^2 which falls between the B3LYP-D3(BJ)/cc-pVQZ estimated values for the equilibrium structure (2.86 amu Å^2) (Table 1) and the heavy atom planar transition state (1.53 amu Å^2). Interestingly, the latter is nearly identical to that of the lowest energy conformer of allyl-NC (1.50 amu Å^2)[42] with a backbone similar to that of allyl-NCS conformer II (1.55 amu Å^2) which suggests that this value describes the out-of-plane contributions from the methylene H atoms.

As noted above, beyond the θ coordinate that interconverts the conformer Ia/Ib pair, the remaining geometric parameters in Table 4 for allyl-NCS are strikingly similar which affords the opportunity to look for structural trends among related molecules. Comparison of the r_0 structures of allyl-NCS and allyl-NCO in Table 4 shows that the nature of the chalcogen atom does not significantly alter the geometry of the allyl segment of the molecule despite the fact that conformer I is stabilized by an interaction between the allyl and iso(thio)cyanato fragments. This is consistent with the previously reported geometries of phenyl-NCO and phenyl-NCS which found no differences in the electronic structure of the ring backbone despite the possibility of a change in π-delocalization of the ring with added -NCO or -NCS substituents.[19] The terminal chalcogen atom does, however, influence the geometry around nitrogen as observed from the ~15^{o} increase in the C_4-N-C_3 bond angle upon replacing oxygen with sulfur. The increased angle around nitrogen in allyl-NCS is accompanied by a decrease in the C4-N and N-C3 r_e bond lengths. Similar structural changes are observed in other R-NCO and R-NCS species with the R=allyl results in this work

being most similar to those reported for R=cyano in which the C-N-C angle increases by 14° in NCNCS[43] relative to the value in NCNCO.[44] The effect is larger than that reported for R=phenyl (9.9°),[19] H (8°)[45,46] and R= CH_3 (7.5°).[47]

To better comprehend the underlying reasons for the observed changes in geometry, the electronic environment around nitrogen was investigated using the results from natural bond orbital (NBO) analysis for conformers I of allyl-NCO[11] and allyl-NCS. Comparison of the σ-bonding framework around nitrogen reveals that the hybridization of nitrogen is ~$sp^{1.5}$ in allyl-NCO and more sp-like in allyl-NCS which is consistent with the larger C_4-N-C_3 angle in the latter. This ~sp-hybridization implies that the CN portion of the isothiocyanato fragment has more triple bond character which is confirmed by the presence of two occupied π-bonding orbitals between C4 and N in the NBO results and by the absence of an orbital consistent with lone pair electron character on nitrogen. In the isovalent allyl-NCO analogue, on the other hand, there is an orbital that is best described as a nitrogen lone pair and only one π-bond between C4 and N as one would expect for a fragment that more closely approximates sp^2-like hybridization at nitrogen. The variation in electronic structure around nitrogen in allyl-NCO and allyl-NCS is comparable in nature to the trend reported in Ph-NCO and Ph-NCS,[19] although more pronounced when R=allyl. A careful inspection of the orbitals involving nitrogen in Ph-NCS and allyl-NCS show that in the former, one of the π-bonds (C4-N) is primarily localized on N (85%) and thus more closely resembles lone pair character than its counterpart in allyl-NCS (69%) which is more evenly shared. This subtle difference in the electronic environment surrounding nitrogen manifests in a smaller N-C-N bond angle for Ph-NCS (145.2(2)°) than for allyl-NCS (152.0(3)°).

Finally, the influence of the terminal chalcogen atoms on the electronic structure around nitrogen appears largely driven by the differences in the size and electronegativity of oxygen

versus sulfur. Careful study of the nature of the occupied orbitals in allyl-NCS, for example, reveals that the larger sulfur atom has three lone pairs of electrons and forms a single σ-bond with the adjacent C4. In allyl-NCO,[11] in contrast, a π-bond is also formed between the more similarly-sized oxygen and C4 atoms leaving only two lone pairs of electrons on the terminal chalcogen. The NBO results are somewhat surprising, however, as the derived bond lengths for C4-S (1.583(4) Å) and C4-O (1.171(13) Å) in Table 4 are more consistent with typical double bonds C=S (1.60 Å) and C=O (1.20 Å) in these fragments.

Conclusion

In summary, the conformational landscape of allyl-NCS was examined FTMW spectroscopy in concert with dispersion-corrected DFT and *ab initio* quantum chemical methods. When dispersion interactions are accounted for, a new global minimum is predicted and this new conformer I was observed experimentally for the first time in this work. This reinforces the importance of including dispersion effects when studying conformational space.[37] The geometry of conformer I derived from the experimental rotational constants is consistent with the accompanying potential energy landscape that permits conformer I to undergo large amplitude motions in the θ coordinate to interconvert the enantiomeric pair Ia/Ib. Upon comparison of the geometry of conformer I with that of allyl-NCO, the largest difference observed is the increase in the C-N-C angle in changing the terminal chalcogen atom from oxygen to sulfur. This is explained via the accompanying NBO results which reveal that the hybridization of nitrogen is more ~sp in nature in allyl-NCS compared with ~$sp^{1.5}$ in allyl-NCO.[11] This is consistent with differences in bonding stemming from the disparate sizes and electronegativities of the terminal chalcogen atoms. The differences in the geometry around nitrogen are more pronounced in the allyl-

substituted species than those reported for other R-NCO and R-NCS pairs where R=phenyl,[19] methyl[47] and H.[45,46] This confirms that the orbital character of the adjacent organic fragment is also a key factor that influences the electronic environment at the nitrogen link in this class of molecules.

Supporting information

Appendix I: Comparison of Basis Sets Used to Estimate Spectroscopic Constants of Allyl-NCS at the B3LYP-D3BJ Level.

Appendix II: Observed Transitions of Allyl-NCS Conformers I and III.

Appendix III: Ground State Effective (r_0) Geometry and Atomic Coordinates (Å) Used to Derive the Ground State Effective Geometry of Allyl-NCS Conformer I.

Appendix IV: Kraitchman Coordinates (Å) Used to Derive the Substitution Structure of Allyl-NCS Conformer I.

Appendix V: Calculated Atomic Coordinates (Å) in the Principal Axis System for the Equilibrium Geometry of Conformer I and the Transition State for the Interconversion of Ia/Ib.

Appendix VI: Transition State Geometries for the Interconversion Pathway Between the Enantiomeric Forms of Conformer I.

Appendix VII: Diagonalization of Nuclear Quadrupole Coupling Tensors of Conformers I of Allyl-NCS and Allyl-NCO.

Additionally, the fit files from SPFIT for all isotopologues of conformers I and III and the Gaussian output data (generated with the ESIgen program[48]) are provided as text files.

Acknowledgements

We thank Professors Yunjie Xu and Jens-Uwe Grabow for interesting discussions about large amplitude motions. This research is funded by the Natural Sciences and Engineering Research Council of Canada (NSERC) through the Discovery Grant program and the University of Manitoba for providing access to its advanced research computing resource, Grex. W. Silva is grateful for financial support provided through the UM Graduate Fellowship (UMGF) program of the Faculty of Graduate Studies of the University of Manitoba.

References

(1) Snyder, L. E.; Buhl; D. Interstellar Methylacetylene and Isocyanic Acid. *Nat. Phys. Sci.* **1973**, *243* (125), 45–46.

(2) Frerking, M. A.; Linke, R. A.; Thaddeus, P. Interstellar Isothiocyanic Acid. *Astrophys. J.* **1979**, *234*, L143–L145.

(3) Brünken, S.; Belloche, A.; Martín, S.; Verheyen, L.; Menten, K. M. Interstellar HOCN in the Galactic Center Region. *Astron. Astrophys.* **2010**, *516* (22), 1–8.

(4) Brünken, S.; Gottlieb, C. A.; McCarthy, M. C.; Thaddeus, P. Laboratory Detection of HOCN and Tentative Identification in Sgr B2. *Astrophys. J.* **2009**, *697* (1), 880–885.

(5) Brünken, S.; Yu, Z.; Gottlieb, C. A.; McCarthy, M. C.; Thaddeus, P. Laboratory Detection of Thiocyanic Acid HSCN. *Astrophys. J.* **2009**, *706* (2), 1588–1593.

(6) Halfen, D. T.; Ziurys, L. M.; Brünken, S.; Gottlieb, C. A.; McCarthy, M. C.; Thaddeus, P. Detection of a New Interstellar Molecule: Thiocyanic Acid HSCN. *Astrophys. J.* **2009**, *702* (2), L124–L127.

(7) Halfen, D. T.; Ilyushin, V. V.; Ziurys, L. M. Interstellar Detection of Methyl Isocyanate CH3NCO in Sgr B2(N): A Link From Molecular Clouds to Comets. *Astrophys. J. Lett.* **2015**, *812*, L5.

(8) Cernicharo, J.; Kisiel, Z.; Tercero, B.; Kolesniková, L.; Medvedev, I. R.; López, A.; Fortman, S.; Winnewisser, M.; de Lucia, F. C.; Alonso, J. L.; et al. A Rigorous Detection of Interstellar CH 3 NCO: An Important Missing Species in Astrochemical Networks. *Astron. Astrophys.* **2016**, *587*, L4.

(9) Zhang, Y. Cancer-Preventive Isothiocyanates: Measurement of Human Exposure and Mechanism of Action. *Mutat. Res-Fund. Mol. M.* **2004**, *555* (1–2), 173–190.

(10) Lin, C.-Mi.; Preston, J. F.; Wei, C.-I. Antibacterial Mechanism of Allyl Isothiocyanate. *J. Food. Prot.* **2000**, *63* (6), 727–734.

(11) Sun, W.; Sogeke, O. P.; Silva, W. G. D. P.; van Wijngaarden, J. Dispersion-Driven Conformational Preference in the Gas Phase: Microwave Spectroscopic and Theoretical Study of Allyl Isocyanate. *J. Chem. Phys.* **2019**, *151* (19), 194304.

(12) Maiti, S.; Jaman, A. I.; Nandi, R. N. Microwave Spectrum of Allyl Isocyanate: Gauche Conformer. *J. Mol. Spectrosc.* **1993**, *158* (1), 8–13.

(13) Jaman, A. I.; Bangal, P. R. Millimeter-Wave Spectrum and Ab Initio DFT Calculation of the C-Gauche Conformer of Allyl Isocyanate. *J. Mol. Spectrosc.* **2009**, *255* (2), 134–138.

(14) Maiti, S.; Jaman, A. I.; Nandi, R. N. Microwave Spectrum of Allyl Isothiocyanate: Gauche Conformer. *J. Mol. Spectrosc.* **1994**, *165* (1), 168–172.

(15) Jaman, A. I. Centrifugal Distortion Analysis of the Microwave Spectrum of Allyl Isothiocyanate (C-Gauche Conformer). *PRAMANA-J. Phys.* **1999**, *53* (5), 857–862.

(16) Glaser, R.; Hillebrand, R.; Wycoff, W.; Camasta, C.; Gates, K. S. Near-Silence of Isothiocyanate Carbon in 13C NMR Spectra: A Case Study of Allyl Isothiocyanate. *J. Org. Chem.* **2015**, *80* (9), 4360–4369.

(17) Ross, S. C.; Cooper, T. A.; Firth, S.; Kroto, H. W.; Walton, D. R. M. The Microwave Spectrum and Semirigid Bender Analysis of Isocyanatoethyne, HCCNCO. *J. Mol. Spectrosc.* **1992**, *152*, 152–167.

(18) Sun, W.; Davis, R. L.; Thorwirth, S.; Harding, M. E.; van Wijngaarden, J. A Highly Flexible Molecule: The Peculiar Case of Ethynyl Isothiocyanate HCCNCS. *J. Chem. Phys.* **2018**, *149*, 104304.

(19) Sun, W.; Silva, W. G. D. P.; van Wijngaarden, J. Rotational Spectra and Structures of Phenyl Isocyanate and Phenyl Isothiocyanate. *J. Phys. Chem. A.* **2019**, *123*, 2351–2360.

(20) Sedo, G.; van Wijngaarden, J. Fourier Transform Microwave Spectra of a New Isomer of OCS-CO2. *J. Chem. Phys.* **2009**, *131*, 44303.

(21) Evangelisti, L.; Sedo, G.; van Wijngaarden, J. Rotational Spectrum of 1,1,1-Trifluoro-2-Butanone Using Chirped-Pulse Fourier Transform Microwave Spectroscopy. *J. Phys. Chem. A.* **2011**, *115* (5), 685–690.

(22) Møller, C.; Plesset, M. S. Note on an Approximation Treatment for Many-Electron Systems. *Phys. Rev.* **1934**, *46* (7), 618–622.

(23) Frisch, M. J.; Trucks, G. W.; Schlegel, H. B.; Scuseria, G. E.; Robb, M. A.; Cheeseman, J. R.; Scalmani, G.; Barone, V.; Petersson, G. A.; Nakatsuji, H.; et al. *Gaussian 16*, Revision B.01; Gaussian, Inc.: Wallingford, CT 2016.

(24) Becke, A. D. Density-Functional Exchange-Energy Approximation with Correct Asymptotic Behavior. *Phys. Rev. A* **1988**, *38* (6), 3098–3100.

(25) Lee, C.; Yang, W.; Parr, R. G. Development of the Colle-Salvetti Correlation-Energy Formula into a Functional of the Electron Density. *Phys. Rev. B* **1988**, *37* (2), 785–789.

(26) Grimme, S.; Ehrlich, S.; Goerigk, L. Effect of the Damping Function in Dispersion Corrected Density Functional Theory. *J. Comput. Chem.* **2011**, *32* (7), 1456–1465.

(27) Becke, A. D.; Johnson, E. R. A Density-Functional Model of the Dispersion Interaction. *J. Chem. Phys.* **2005**, *123* (15), 154101.

(28) Dunning, T. H. Gaussian Basis Sets for Use in Correlated Molecular Calculations. V. Core-valence Basis Sets for Boron through Neon. *J. Chem. Phys.* **1989**, *90* (2), 1007–1023.

(29) Kendall, R. A.; Dunning, T. H.; Harrison, R. J. Electron Affinities of the First-row Atoms Revisited. Systematic Basis Sets and Wave Functions. *J. Chem. Phys.* **1992**, *96* (9), 6796–6806.

(30) Woon, D. E.; Dunning, T. H. Gaussian Basis Sets for Use in Correlated Molecular Calculations. III. The Atoms Aluminum through Argon. *J. Chem. Phys.* **1993**, *98* (2), 1358–1371.

(31) Glendening, E. D. .; Badenhoop, J. K. .; Reed, A. E. .; Carpenter, J. E. .; Bohmann, J. A. .; Morales, C. M. .; Landis, C. R. .; Weinhold, F. *NBO* 6.0; Theoretical Chemistry Institute, University of Wisconsin, Madison, WI 2013.

(32) Pickett, H. M. The Fitting and Prediction of Vibration-Rotation Spectra with Spin Interactions. *J. Mol. Spectrosc.* **1991**, *148* (2), 371–377.

(33) Watson, J. K. G. *Vibration Spectra and Structure*: *A Series of Advances*; Durig, J. R.; Ed.; Elsevier: New York, 1977; Vol. *6*, pp 1-89.

(34) Kisiel, Z. PROSPE - Programs for ROtational SPEctroscopy http://www.ifpan.edu.pl/~kisiel/prospe.htm (accessed Feb 3, 2020).

(35) Kraitchman, J. Determination of Molecular Structure from Microwave Spectroscopic Data. *Am. J. Phys.* **1953**, *21* (1), 17–24.

(36) Costain, C. C. *Further Comments on the Accuracy of r_s Substitution Structures*; Bradley, W. F.; Hanson, H. P.; Eds.; Transactions of the American Crystallographic Association: Austin, 1966; Vol. 2, pp 157-163.

(37) Uriarte, I.; Insausti, A.; Cocinero, E. J.; Jabri, A.; Kleiner, I.; Mouhib, H.; Alkorta, I. Competing Dispersive Interactions: From Small Energy Differences to Large Structural Effects in Methyl Jasmonate and Zingerone. *J. Phys. Chem. Lett.* **2018**, *9* (20), 5906–5914.

(38) Chrostowska, A.; Darrigan, C.; Dargelos, A.; Graciaa, A.; Guillemin, J. C. Isoselenocyanates versus Isothiocyanates and Isocyanates. *J. Phys. Chem. A* **2018**, *122* (11), 2894–2905.

(39) Ruoff, R. S.; Klots, T. D.; Emilsson, T.; Gutowsky, H. S. Relaxation of Conformers and Isomers in Seeded Supersonic Jets of Inert Gases. *J. Chem. Phys.* **1990**, *93* (5), 3142–3150.

(40) Xie, F.; Seifert, N. A.; Heger, M.; Thomas, J.; Jäger, W.; Xu, Y. The Rich Conformational Landscape of Perillyl Alcohol Revealed by Broadband Rotational Spectroscopy and Theoretical Modelling. *Phys. Chem. Chem. Phys.* **2019**, *21* (28), 15408–15416.

(41) Huang, W.; Thomas, J.; Jäger, W.; Xu, Y. Tunnelling and Barrier-Less Motions in the 2-Fluoroethanol–Water Complex: A Rotational Spectroscopic and Ab Initio Study. *Phys. Chem. Chem. Phys.* **2017**, *19* (19), 12221–12228.

(42) Haykal, I.; Margulès, L.; Huet, T. R.; Motyienko, R. A.; Écija, P.; Cocinero, E. J.; Basterretxea, F.; Fernández, J. A.; Castaño, F.; Lesarri, A.; et al. The CM-, MM-, and SUB-MM-WAVE Spectrum of Allyl Isocyanide and Radioastronomical Observations in Orion KL and the SgrB2 Line Surveys. *Astrophys. J.* **2013**, *777* (2), 2–9.

(43) King, M. A.; Kroto, H. W.; Landsberg, B. M. Microwave Spectrum of the Quasilinear Molecule, Cyanogen Isothiocyanate (NCNCS). *J. Mol. Spectrosc.* **1985**, *113* (1), 1–20.

(44) Hocking, W. H.; Gerry, M. C. L. The Microwave Spectrum of Cyanogen Isocyanate (NCNCO). *J. Mol. Spectrosc.* **1976**, *59* (3), 338–354.

(45) Hocking, W. H.; Gerry, M. C. L.; Winnewisser, G. The Microwave and Millimetre Wave Spectrum, Molecular Constants, Dipole Moment, and Structure of Isocyanic Acid, HNCO. *Can. J. Phys.* **1975**, *53* (19), 1869–1901.

(46) Beard, C. I.; Dailey, B. P. The Structure and Dipole Moment of Isothiocyanic Acid. *J. Chem. Phys.* **1950**, *18* (11), 1437–1441.

(47) Lett, R. G.; Flygare, W. H. Microwave Spectrum, Barrier to Internal Rotation, 14 N Nuclear Quadrupole Interaction, and Normal-Coordinate Analysis in Methylisocyanate, Methylisothiocyanate, and Methylthiocyanate. *J. Chem. Phys.* **1967**, *47* (11), 4730–4750.

(48) Rodríguez-Guerra Pedregal, J.; Gómez-Orellana, P.; Maréchal, J.-D. ESIgen: Electronic Supporting Information Generator for Computational Chemistry Publications. *J. Chem. Inf. Model.* **2018**, *58* (3), 561–564.

TOC graphic

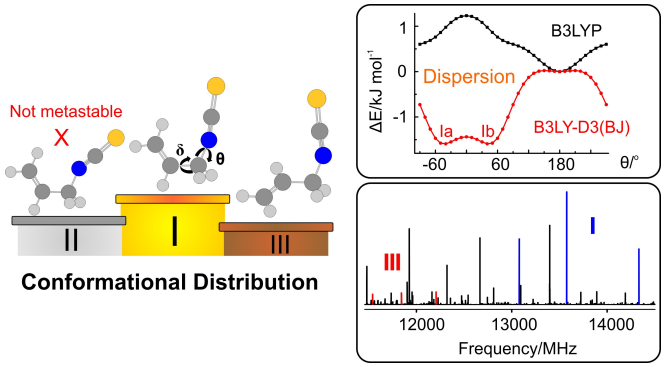
Not metastable
X
δ
θ
II
I
III
Conformational Distribution
1
0
-1
ΔE/kJ mol⁻¹
B3LYP
Dispersion
Ia
Ib
B3LY-D3(BJ)
-60
60
180
θ/°
III
I
12000
13000
14000
Frequency/MHz